ACS APPLIED ENERGY MATERIALS

www.acsaem.org Article

Cobalt Hexacyanoferrate as a Selective and High Current Density Formate Oxidation Electrocatalyst

Lijuan Han, Jesús González-Cobos, Irene Sánchez-Molina, Stefano Giancola, Scott J. Folkman, Pengyi Tang, Marc Heggen, Rafal E. Dunin-Borkowski, Jordi Arbiol, Sixto Giménez, and Jose Ramon Galan-Mascaros*

Cite This: *ACS Appl. Energy Mater.* 2020, 3, 9198–9207 Read Online

ACCESS | Metrics & More | Article Recommendations | Supporting Information

ABSTRACT: Herein we report the selectivity, stability, and electrochemical characterization of cobalt hexacyanoferrate, the Co–Fe Prussian Blue derivative (CoFePB), as a formate/formic acid oxidation electrocatalyst in aqueous media. CoFePB is able to quantitatively catalyze (100% Faradaic efficiency within less than 8% standard error at pH 5) the electrochemical oxidation of formate to CO_2 over a pH range of 1–13. This quantitative formate elecrooxidation is possible due to the exclusive selectivity of the catalyst in a wide potential window (from *ca.* 1.2 to 1.7 V *vs* RHE), where no other substrate in aqueous conditions is activated: neither other organic molecules, such as alcohols or acids, nor water itself. CoFePB is one of the first heterogeneous noble-metal-free catalysts reported for the electrooxidation of small hydrocarbon molecules. Importantly, the catalyst showed a very high tolerance against surface poisoning during the reaction, as supported by the cyclic voltammetry and electrochemical impedance spectroscopy data, thereby allowing CoFePB to operate at greater current density than state-of-the-art noble metal catalysts. For example, we observed that CoFePB is able to achieve a formate oxidation current ~10 mA cm^{-2} at pH 5, 0.4 M formate at 1.4 V *vs* RHE, whereas a Pt disk and Pd(5%)/C electrodes had currents of 0.4 and 1.4 mA cm^{-2}, respectively, under identical conditions. The remarkable selectivity, stability, and high current density of CoFePB, in contrast to state-of-the-art catalysts based on platinum-group metals, is an important step in the search for inexpensive earth-abundant materials for oxidation of organic molecules for use in liquid fuel cells or for selective organic molecule sensors. Furthermore, because CoFePB is not poisoned by intermediates and can achieve higher current density than Pt or Pd, improvement of the catalyst onset potential can lead to higher power density formate oxidation fuel cells using earth-abundant metals than with Pt or Pd.

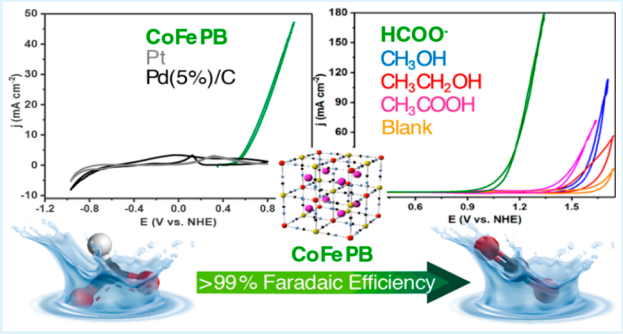

KEYWORDS: *electrocatalysis, formate/formic acid oxidation, electrochemical impedance spectroscopy (EIS), cobalt hexacyanoferrate, liquid fuel cells*

INTRODUCTION

The selective electrochemical oxidation of small organic molecules is getting attention for multiple applications, including sensing and analysis, environmental remediation, and energy-related systems, such as fuel cells. In the latter sense, liquid hydrogen carriers (alcohols, acids, and sugars) have been proposed as potential H_2 storage media, given their high volumetric energy density and ease of transport, handling and storage.[1−6] Furthermore, direct liquid fuel cells could be an alternative, more practical system compared to hydrogen fuel cells. In particular, direct formic acid fuel cells or direct formate fuel cells present higher theoretical cell voltage than fuel cells running on methanol or ethanol. Additionally, formate can be produced from CO_2 reduction by renewable energy sources, thereby forming a carbon-neutral fuel cycle.[7,8] Formate is also highly soluble in water, thereby avoiding flammable organic solvents and leading to safer operation. Regarding the sensing field, selective formate/formic acid electrooxidation materials are important, for instance, in analysis of pollutants in the atmosphere and natural waters, detection of liquid fuel cell crossover, or control of aerobic and anaerobic fermentation processes.[9−12]

Electrooxidation catalysts for small organic molecules are typically nonselective and mostly based on noble metals or platinum-group metals (PGMs) such as Pt or Pd. Furthermore, these catalysts may be subject to poisoning by intermediate

Received: July 1, 2020
Accepted: August 11, 2020
Published: August 31, 2020

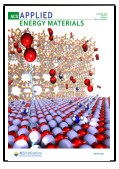

https://dx.doi.org/10.1021/acsaem.0c01548
ACS Appl. Energy Mater. 2020, 3, 9198–9207

products or impurities.[13,14] Noble-metal-free electrocatalysts toward the anodic oxidation of small hydrocarbon molecules are scarce.[1,15] Thus, we are interested in catalysts made of earth-abundant materials for the selective aqueous oxidation of formate/formic acid. There are few studies on $HCOO^-$/HCOOH electrooxidation where some transition metals are employed in conjunction with Pd or Pt.[16−19] To our knowledge, there is only one work, from Bisht *et al.*,[20] where a fully noble-metal-free catalyst is employed. In this study, the authors tested a perovskite-type catalyst, $La_{0.8}Sr_{0.2}CoO_3$, in a 0.5 M KNO_3 electrolyte solution containing HCOOH (2.1 M) and, interestingly, they observed some formic acid oxidation even under open circuit conditions, which was attributed to the contribution of lattice oxygen. However, the reaction rate in these conditions was sluggish and only reached a maximum of ~2 mA cm^{-2} at 1.4 V *vs* RHE. There are a few more non-noble metal catalysts for formic acid oxidation, but they work under very limited conditions. For example, dehydrogenase enzymes are very sensitive to temperature, pH, and so on and lack long-term stability.[21,22] The only synthetic homogeneous electrocatalysts with high activity toward formate oxidation, the family of $[Ni(PR_2NRO_2)_2(CH_3CN)]^{2+}$ catalysts,[23,24] can only work in ultrapure organic solvents and are sensitive to trace amounts of water, air, or other impurities.

As a plausible oxidation catalyst for organic substrates, we investigated cobalt hexacyanoferrate (CoFePB), a versatile and robust oxidation catalyst in a wide pH range, with a proven performance in water oxidation (photo)electrocatalysis.[25−28] In the present work we have found that CoFePB offers excellent selectivity and efficiency toward aqueous $HCOO^-$ oxidation under a range of pH 1−13. Its performance was evaluated electrochemically and has been compared with that of state-of-the-art catalysts, also providing mechanistic insights on the reaction kinetics. To our knowledge, CoFePB is the first earth-abundant heterogeneous electrocatalyst for the selective oxidation of formate/formic acid in water and is unique when compared to the commonly used but expensive Pt- or Pd-based catalysts.

EXPERIMENTAL SECTION

Materials and Chemicals. All chemicals used were analytical reagent grade, and included cobalt(II) nitrate hexahydrate $Co(NO_3)_2 \cdot 6H_2O$ (Aldrich), urea (98% CH_4NO_2; Aldrich), potassium hexacyanoferrate ($K_3Fe(CN)_6$;Aldrich), 98% formic acid solution (Aldrich), 63−67% nitric acid (Aldrich), and 98% sulfuric acid (Aldrich). All solutions were prepared using 18.2 MΩ·cm Milli-Q water. If not specified, all commercially available reagents and solvents were used as received without further purification.

Fluorine-doped tin oxide (FTO) coated glass slides (12−14 Ω per square surface resistivity) were purchased from Pilkington NSG TEC 15A 2.2 mm slides with 80.0−81.5% transmittance. Pt foil (99.95%, 0.1 mm thickness) was purchased from Goodfellow. FAA-3 anionic binder (5% solution) was purchased from Fumatech.

Electrode Preparation. The CoFePB electrodes were prepared following a typical synthetic procedure[25] where a thin pink film of CoO_x with a 1 × 1 cm^2 geometric surface area was initially grown on a transparent FTO surface by a hydrothermal method. The CoO_x/FTO sample was subsequently placed in the freshly prepared 800 mg/100 mL $K_3Fe(CN)_6$ aqueous solution and heated at 60 °C for 24 h. Finally, the CoFePB sample was immersed in the concentrated H_2SO_4 solution (pH 1) for more than 4 h to remove any possible remaining traces of oxide and then rinsed with Milli-Q water. The average CoFePB mass loading on the electrodes is 0.3 mg cm^{-2}.

The structure of the CoFePB electrodes was characterized by means of aberration-corrected scanning transmission electron microscopy (STEM) in high-angle annular dark-field (HAADF) mode. From the atomic resolution HAADF STEM images acquired we obtained fast Fourier transform (FFT) power spectra in selected regions and indexed the patterns, which indicated that the obtained sample structure was in good agreement with the $Co_4[Fe(CN)_6]_{2.67} \cdot H_2O_{15.33}$ crystal phase.[25] Additional electron energy-loss spectroscopy (EELS) chemical composition maps were also obtained, corroborating the above composition (Figures 1 and Supporting Information Figures S1 and S2).

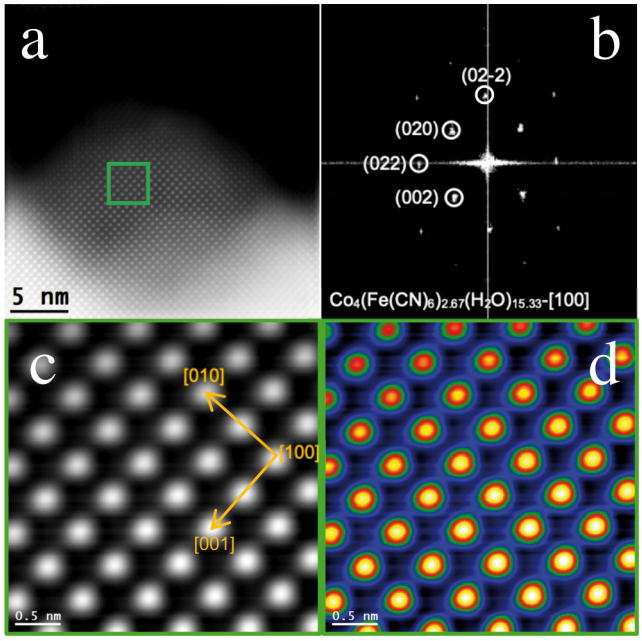

Figure 1. (a) Atomic resolution HAADF STEM image showing the edge of a nanocube. (b) Respective power spectrum (FFT) confirming that the nanocube structure is in agreement with the $Co_4(Fe(CN)_6)_{2.67}(H_2O)_{15.33}$ (FM3-M; space group, 225) crystal phase in the [100] direction. (c, d) Enlarged image from the green squared section in both gray and temperature colored scales.

For comparison purposes, a commercial Pt disk electrode (0.07 cm^2 geometric area) and a carbon-supported Pd catalyst with 5% metal content deposited on FTO (1 × 1 cm^2 geometric area) were also electrochemically tested. The Pd(5%)/C ink was prepared by a procedure adapted from the literature[29] by mixing 30 mg of commercially available Pd(5%)/Vulcan carbon with 25 μL of 5% FAA-3 anionic binder and 9.75 mL of a 3:1 EtOH/water solution and sonicating for 30 min. FTO coated glass slides were cut into 3 × 1 cm^2 strips, then sonicated in a soap water solution for 10 min, rinsed thoroughly with distilled water, sonicated in ethanol for 10 min, rinsed thoroughly with ethanol, and finally sonicated in acetone for 10 min before allowing to air-dry. The Pd(5%)/C ink was then sprayed onto the FTO substrate that had been masked with Kapton tape to expose only a 1 × 1 cm^2 surface area on a hot plate heated to 80 °C. The electrode was weighed before and after the coating to obtain the mass of added catalyst and was typically between 1.5 and 2 mg of Pd(5%)/C per 1 cm^2 electrode surface area.

Electrochemical Methods. All electrochemical experiments were conducted under ambient conditions, with a computer-controlled Bio-Logic VMP3 multichannel potentiostat. In order to maintain a constant ionic strength, 1 M KNO_3 was added to reduce the impact stemmed from mass diffusion and to ensure a good ionic conductivity. The pH was adjusted by adding aliquots of concentrated KOH or HNO_3. The total electrolyte volume was 30 mL.

For our study, we employed a standard three-electrode arrangement with a Pt mesh counter electrode and a saturated calomel electrode (SCE) as reference electrode. The potentiodynamic

https://dx.doi.org/10.1021/acsaem.0c01548
ACS Appl. Energy Mater. 2020, 3, 9198−9207

polarization curves were recorded at a scan rate of 20 mV s^{-1} without magnetic stirring, while the quasi-steady-state polarization curves were measured at a sweep rate of 5 mV s^{-1} under magnetic stirring. Chronoamperometric measurements (CA) were conducted at a constant applied potential under vigorous stirring in a H-shaped cell with medium porosity glass frits. Steady-state current densities for Tafel analyses were collected at a variety of applied potentials within formate electrocatalytic oxidation windows. Working potential was swept from low to high values with 40 mV increments. At each potential, the current was stabilized for 10 min to attain a steady-state value with the stirred solution (600 rpm). All potentials reported in this work are expressed *vs* RHE unless otherwise indicated by adding +0.241 V and +0.059 pH to the potential *vs* SCE. Current densities are always normalized to the corresponding geometric surface area.

CO_2 Evolution Efficiency. The theoretical CO_2 amount was calculated from the total amount of charge (Q) passed through the electrode during CA measurements, taking into account that two electrons are required to produce one CO_2 molecule. The experimental amount of CO_2 produced was quantitatively determined by using a calibrated mass spectrometer (MS). Mass-to-charge ratios (m/z) of 2, 12, 14, 16, 17, 18, 22, 28, 30, 32, 44, 46, and 47 were continuously monitored with a quadrupole mass spectrometer (Pfeifer OmniStar GSD 301 C) during different chronopotentiometries carried out in the three-electrode cell under N_2 bubbling (50 N mL min^{-1}). The experimental flows were estimated from the MS signals obtained for m/z = 22 and 44, which were previously calibrated with certified standards (Air Liquide) of CO_2 (99.999% purity and 1.5% N_2), and the N_2 flow was controlled by a mass flowmeter (Bronkhorst EL-FLOW).

A chronoamperometry experiment was also performed without N_2 flow through the cell in order to perform static analysis of the headspace (volume of 23 N mL) with an Agilent 7820A gas chromatography (GC) system equipped with columns Washed Molecular Sieve 5A, 2 m × 1/8 in. OD, Mesh 60/80 SS and Porapak Q, 4 m × 1/8 in. OD, SS, Mesh 80/100 SS, and a thermal conductivity detector. ^{1}H and ^{13}C-NMR (nuclear magnetic resonance) experiments were performed in a Bruker 300 MHz spectrometer at room temperature. For sample preparation, 250 μL of the mother anolyte was extracted from the electrochemical cell with a microsyringe and placed in a vial. Then, 250 μL of a stock solution of ascorbic acid and 0.4 M in D_2O were added, and the sample was passed to the NMR tube for measurement.

Electrochemical AC Impedance Spectroscopy. Electrochemical impedance spectroscopy (EIS) was performed by means of a typical three-electrode cell in the frequency range from 100 kHz to 0.1 Hz with 8 points per decade. The AC perturbation was 5 mV.

Characterization Methods. The chemical composition and the structure of the compounds were characterized by infrared transmittance spectra (FTIR-ATR Cary 630 TR1 Ph2) and Raman spectroscopy (Renishaw in Via Reflex Raman confocal microscope, Gloucester- Shire, U.K.; light source, 514 nm). Scanning electron microscopy (SEM) micrographs were acquired using an FEI Quanta 650 FEG ESEM at 20 kV equipped with an Oxford EDX analyzer (Oxford Instruments). Atomic resolution AC HAADF STEM and further EELS-STEM analyses were conducted at the FEI TITAN G3 50-300 PICO operated at 80 kV. Images have been analyzed using the DigitalMicrograph (Gatan Inc., USA) software package.

RESULTS AND DISCUSSION

Formate Electrooxidation on CoFePB. The oxidation performace of CoFePB was initially investigated at two different pHs, 5 and 13, *via* cyclic voltammetry (CV) of a 0.4 M formate solution in 1 M KNO_3 electrolyte (Figure 2). A characteristic formate oxidation wave appears at *ca.* 1.2 V *vs* RHE at both pH 5 and 13, respectively. In the first case, this onset potential is below the reversible Co^{II}/Co^{III} redox couple in CoFePB, *ca.* 1.5 V *vs* RHE (see inset of Figure 2a), and in the latter case both potentials are fairly overlapping, since the

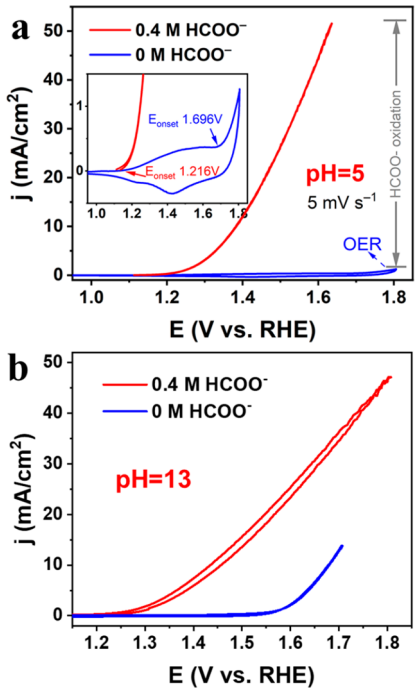

Figure 2. Cyclic voltammograms (CVs) on CoFePB electrodes in (a) pH 5 and (b) pH 13 aqueous solutions in the presence (red line) and absence (blue line) of 0.4 M $HCOO^-$. Electrolyte, 1 M KNO_3. Scan rate, 5 mV s^{-1}. Note, oxidation waves that are typical of formate oxidation with Pt or Pd are not observed here because CoFePB has a different electrochemical mechanism, *vide infra*.

Co^{II}/Co^{III} redox potential is *ca.* 1.17 V *vs* RHE at pH 13.[25] At both pH values, the onset of formate oxidation is well below the oxygen evolution reaction (OER) onset potential, which is *ca.* 1.7 and 1.57 V *vs* RHE at pH 5 and 13, respectively. Therefore, the contribution of OER to the observed current can be considered minimal, consistent with our observed Faradaic efficiency (*vide infra*).

If we compare the results obtained at both pH values, the formate oxidation onset potential decreases with pH at 61 mV/pH. Such pH dependence is expected since formic/formate oxidation reaction will release protons as product, as shown in eq 1:

$$HCOOH \rightarrow CO_2 + 2H^+ + 2e^- \qquad E_0 = -0.20\ V \tag{1}$$

In terms of overpotential (η), it can be observed that the electrocatalytic activity of CoFePB is almost pH independent, with an onset of *ca.* 1.4 V *vs* the thermodynamic potential of formate oxidation in both pH conditions. Similar conclusions were obtained in preliminary experiments with 0.4 M formate/formic solution in 1 M KNO_3 electrolyte and 0.1 KPi buffer, which were carried out in a pH range from 1 to 13 (Figure S3). The current observed in the presence of KPi was lower than in its absence, indicating an inhibitory effect of the phosphate anion on the catalysis, as confirmed by control experiments in the presence and absence of KPi (Figure S4). We hypothesize that this could be attributed to partial blocking of the catalytic sites and/or to displacement of reactive intermediate species by the weak adsorption of phosphate anions.

The linear pH dependence of the onset potential suggests that CoFePB is active toward the oxidation of formate over a wide pH range of 1−13 (Figure S3). Furthermore, current

https://dx.doi.org/10.1021/acsaem.0c01548
ACS Appl. Energy Mater. 2020, 3, 9198−9207

densities were consistent in all pH ranges studied, indicating negligible poisoning effect of OH^- ions on the active electrocatalytic sites. This is particularly relevant since OH^- anions are known to hinder the catalytic oxidation of small molecules oxidation, for example, in Pt-based systems where severe poisoning above pH 11 has been reported.[30−33]

We then examined the effect of formate concentration in alkaline, pH 13 and near-neutral, pH 5 conditions where maximum currents and minimum overpotentials were observed, respectively. Figure 3a shows the anodic polarization

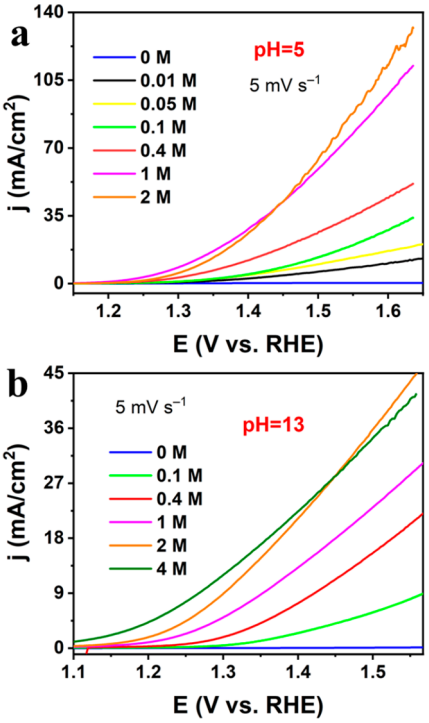

Figure 3. Anodic polarization data on CoFePB electrodes in 1 M KNO_3 aquesous electrolyte at 5 mV/s scan rates. Current density as a function of $[HCOO^-]$ at (a) pH 5 and (b) pH 13.

voltammograms for CoFePB electrodes in pH 5 KNO_3 (1 M), as a function of formate concentration (up to 2 M) with a scan rate of 5 mV/s. The presence of the formate oxidation wave is detected from low concentrations (10 mM) with the appearance of anodic current with *ca.* 1.2 V onset potential. The anodic current increases with concentration, reaching saturation at formate concentration above 1 M. Analogous results were found at pH 13 (Figure 3b), although higher concentration is needed to reach maximum current (>2 M).

For both pH 5 and 13 the electrochemical current is nearly identical when comparing anodic and cathodic sweeps at 5 mV/s, indicating pseudo-steady-state reaction kinetics and, importantly, providing evidence against the catalyst poisoning by intermediates (Figure S5). This apparent absence of hysteresis between positive and negative scans indicates a negligible inhibition rate or a low tendency toward surface poisoning under these conditions (on this time scale and potential range), in contrast with the poisoning by CO_{ads} species taking place on Pt-based electrocatalysts[32,34] and, to a lesser extent, on Pd-based electrocatalysts.[17,35]

Selectivity of CoFePB to Formate Oxidation. Regarding product selectivity, we analyzed the distribution of gaseous products during formate electro-oxidation at 1.49 V *vs* RHE at pH 5 (chronoamperometry shown in Figure S6b). By means of gas chromatography, only CO_2 gas was detected, apart from nitrogen, used to initially deaerate the cell headspace volume, and oxygen amounts similar to those found when injecting N_2 blank samples. No signals from other gaseous species were found. It is worthy to note the absence of CO, which is a common byproduct from the competing dehydration process. We did monitor quantitatively the CO_2 production in the cell headspace by mass spectrometry at pH 5, assisted by continuous flow of N_2 carrier gas through the cell. We found a Faradaic efficiency toward CO_2 production of 100% (within <8% error) (Table 1). The MS experimental data are shown in detail in Tables S1 and S2. The high solubility of CO_2 in alkaline media (pH 13) did not allow us to easily quantitify CO_2 production under these conditions. We also recorded ^{1}H- and ^{13}C-NMR spectra of the aqueous solutions during the electro-oxidation experiment (Figure S7). No other side products, from more complex coupling reactions during electrooxidation, were detected in the electrolyte solution.

The selectivity of CoFePB toward $HCOO^-$ oxidation was additionally investigated by carrying out analogous aqueous electrolysis, at neutral pH, in the presence of other small organic molecules with standard oxidation potentials in a similar range (eqs 2−4), including methanol, ethanol, and acetic acid (Figure 4).

$$CH_3OH \rightarrow CO_2 + 6H^+ + 6e^- \qquad E_0 = 0.040\ V \tag{2}$$

$$CH_3CH_2OH + 3H_2O \rightarrow 2O_2 + 12H^+ + 12e^- \qquad E_0 = 0.085\ V \tag{3}$$

$$CH_3COOH + 2H_2O \rightarrow 2O_2 + 8H^+ + 8e^- \qquad E_0 = 0.123\ V \tag{4}$$

Interestingly, CoFePB catalytic activity toward these other substrates was found to be very poor, comparatively. Only formate shows a significant anodic current at potentials below 1.6 V *vs* RHE. More importantly, only the formate electro-oxidation starts below the reversible CoFePB oxidation and well below the thermodynamic potential of water oxidation, with all other molecules showing oxidation waves at higher potentials. The difference between the electro-oxidation of formate and the other organic molecules observed with the CoFePB catalyst is comparable with that found in literature with noble metal catalysts. For instance, the obtained onset potential of formic acid oxidation is typically 0.1−0.4 V lower

Table 1. Theoretical *vs* Experimental CO_2 Evolution on CoFePB Electrodes during Different Chronopotentiometries at pH 5, 1 M KNO_3, and 0.4 M Formate

current density/(mA cm^{-2})	5	10	15
theoretical CO_2 flow/(N mL min^{-1})	0.037	0.075	0.112
experimental CO_2 flow/(N mL min^{-1})	0.037 ± 0.003	0.077 ± 0.002	0.113 ± 0.003

https://dx.doi.org/10.1021/acsaem.0c01548
ACS Appl. Energy Mater. 2020, 3, 9198−9207

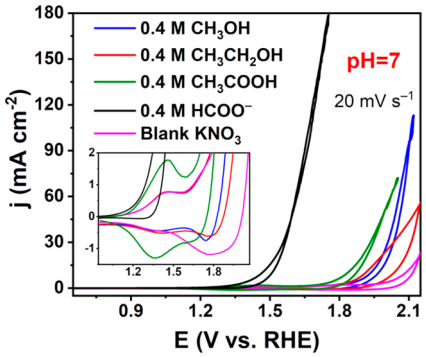

Figure 4. Cyclic voltammograms (20 mV s^{-1}) with a CoFePB working electrode in the presence of small organic molecules (formic acid, methanol, ethanol, and acetic acid) in 1 M KNO_3 aqueous solution at pH 7.

compared to that of methanol or ethanol oxidation with Pt or Pd catalysts,[36−39] while this potential difference is of *ca.* 0.5 V in our case.

The precise reason for this CoFePB selectivity toward formate oxidation (Figure 4) should be related to a different oxidation mechanism. This can be explained either by a simpler reaction pathway since it only involves a two-electron transfer, whereas methanol oxidation to CO_2, for example, would involve a four-electron process along with multiple proton removal and attack by water, or also to the small size and negative charge of formate, making it a good ligand to replace water molecules bound to the active Co^{2+} sites, whereas the rest of the substrates are less prone to substitute bound water molecules, as a first step in the catalytic cycle.

Stability of the CoFePB Electrocatalyst. We also looked into the stability of the CoFePB anodes. The catalytic current density is relatively stable during chronoamperometry (CA) at both pH 5 and pH 13 for several hours (Figure S6). However, there is a small decrease in catalytic current that we hypothesize can be attributed mostly to formate consumption in the finite-volume reaction vessel. For example, at pH 13, with 0.4 M formate the current density decreases from ∼17 to ∼13 mA cm^{-2}, a 24% decrease, whereas the formate depletion (estimated from the average current, multiplied by the full time frame of the experiment, and converted to molar equivlents by the $2e^-$/formate stoichiometry) was approximately 9%. Alternatively, the drop in current could be due to a change in solution pH (or local pH gradient), therefore changing the formal oxidation potential of formate. A drop in pH is posible because the solutions are not buffered and H^+ is generated as a byproduct of formate, so H^+ accumulation is likely. Indeed, assuming that all of the charge passed can be attributed to formate oxidation in the 30 mL cell with $1e^-/H^+$, we estimate that the pH of the solution will change by approximately one pH unit. The other CA experiments in Figure S6 show a similar trend in the decrease in current with small variations in the relative amount of current decrease/substrate consumption—other variations in the CA curves can be related to specific reactions occurring at the counter electrode, among other experimental factors. However, in all cases the substrate depletion and current drop is within a factor of ∼2 meaning that at least half of the current decrease can be accounted for solely from the depletion of formate oxidation.Thus, although we observe a decrease in catalytic current in finite volume (30 mL) setups, we expect to maintain the catalytic current with in flow or by addition of formate when depleted.

Postelectrocatalytic SEM imaging shows no appreciable morphological changes in the CoFePB nanocubes (Figure S8a). Nanocubic shape and microporous structure is preserved without obvious signs of wearing and only showing partial aggregation. We observe small changes in the IR and Raman spectra that could be due to changes in the surface or minor structural changes that do not affect the observed electrocatalysis (Figures S8b,c and S9). Importantly, the catalyst has largely unchanged bands for the CN stretching from the 2100 to 2000 cm^{-1} region. CN stretching is very sensitive to coordination number and the oxidation state of the metal centers,[40,41] and any *in situ* transformation would considerably affect the spectra. Hence, although minor changes are observed in the Raman spectra, the SEM, electrochemistry, and vibrational spectroscopy are all consistent with the conclusion that the bulk of the material remains unchanged during extended electrolysis and no new catalytically active phases are formed.

Comparison with CoO_x and Benchmarking with PGM Electrocatalysts. In oxidation electrocatalysis, it is known that many materials synthesized for catalysis actually serve as precatalysts to other heterogeneous phases formed during the oxidation.[42−45] It can, therefore, be difficult to determine the genuine catalytic activity of a given material. For that purpose, we compared the catalytic activity of a CoO_x film in the same working conditions (Figure S10), as most plausible impurity arising from Co leaching, as observed for several oxidation electocatalysts. No additional oxidation events appeared in the presence of formate, confirming the negligible activity of CoO_x toward this organic compound. This precludes any participation of CoO_x traces in the excellent catalytic activity of CoFePB. Furthermore, we did not observe substantial changes in the electrochemistry during prolonged electrolysis, nor changes in the bulk structure of the CoFePB observed in the electron microscopy or vibrational spectroscopy. All of this evidence taken together provides a strong case that CoFePB is indeed the authentic formate oxidation catalyst.

To benchmark CoFePB as a formate oxidation catalyst, we tested two noble metal catalysts, a Pt disk electrode and a carbon-supported palladium catalyst (Pd(5%)/C), by CV under the same operating conditions, with 0.4 M formate at pH 5 and 13 at a scan rate of 5 mV/s (Figure 5). The overpotential values required for the onset of formate oxidation can be observed in Table 2 and follow the trend of Pd(5%)/C < Pt < CoFePB.[1,39,46]

Another relevant feature from the CVs is the presence of several peaks in both forward and reverse scans on the Pt and Pd catalysts, in the potential range from 0.1 to 1.5 V *vs* RHE at pH 5 and from 0.2 to 1.6 V *vs* RHE at pH 13. The presence of these peaks is consistent with literature on PGM-based catalysts[1,16,18,19,30−34,47−49] and is related to the formate oxidation *via* either a direct or an indirect path (in the latter case through oxidation of adsorbed reaction intermediates) and to the oxidation/reduction of the PGM catalysts. Hence, adsorption of poisoning species such as CO or hydroxyl groups on Pd and Pt leads to very low current densities at high overpotentials, as one can observe in Figure 5 as well as in Table 2 for η = 1.6 V.

In stark contrast to both Pt and Pd(5%)/C, CoFePB displays no significant poisoning effect at high applied potential at any pH (Figures 2, 3, 5, and S3). The continuous increase of

https://dx.doi.org/10.1021/acsaem.0c01548
ACS Appl. Energy Mater. 2020, 3, 9198−9207

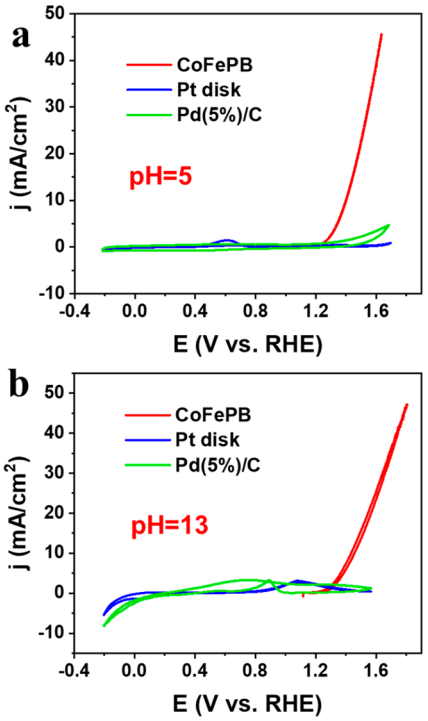

Figure 5. Cyclic voltammograms (5 mV s^{-1}) with CoFePB, Pt, and Pd(5%)/C catalysts (a) pH 5 and (b) pH 13 aqueous solutions containing 0.4 M formate and 1 M KNO_3. CVs of the Pt and Pd catalysts can be observed in more detail in Figure S11.

the current density at high potentials and the absence of any hysteresis denotes that this electrode is not poisoned by adsorbed species contrary to Pt and Pd catalysts. On the other hand, the concurrence of the Co^{2+}/Co^{3+} redox couple at 1.5 and 1.17 V *vs* RHE at pH 5 and 13, respectively, does not passivate the catalyst, which seems to indicate that the oxidized state of CoFePB is the main active phase in the formate oxidation reaction. The implication of this resistance to poisoning and passivation is that CoFePB is a remarkably robust catalyst, since it does not suffer any decrease in current density with these processes, as state-of-the-art Pt and Pd electrodes do.

The results shown herein thus open interesting prospects for the application of CoFePB as a fully noble-metal-free electrocatalyst for the development of direct formate fuel cells (which typically use Pd-based anodes). The performance, however, is presently limited by the onset potential of the formate oxidation which would reduce the operating potential of the fuel cell and hence lower the power efficiency of the device. In order to commercialize an electrode such as CoFePB, the onset potential for formate oxidation would need to be decreased to a value closer to the thermodynamic one while maintaining the high current densities observed herein. Furthermore, the high tolerance against poisoning of CoFePB and its formate oxidation selectivity in a wide range of pH make this material also a promising electrode for formate sensing applications, where the only noble-metal-free sensors reported so far consist of enzymes, which are limited to near-neutral pH conditions.

Reaction Dynamics. Formate half-cell oxidation involves two electron transfers, one C−H bond cleavage, deprotonation, and, probably, adsorbed intermediates. The experimental Tafel plots obtained from steady-state current density show a significant dependence of the Tafel Slope on pH, showing 81 mV dec^{-1} at pH 5 but 130 mV dec^{-1} at pH 13 (Figure S12). This change in Tafel slope indicates a different rate-determing step depending on pH. In detail, the slope at pH 5 is close to 60 mV dec^{-1}, which may be associated with a rate-limited step involving a two-electron transfer. On the contrary, the alkaline Tafel slope near 120 mV dec^{-1} indicates the rate-determing step is more likely to be a 1 e^- transfer in a sequential reaction.[50]

Electrochemical impedance spectroscopy is a helpful technique to understand electrochemical processes, able to distinguish between charge transport, charge transfer, and electrocatalytic contributions to the electrode performance. Representative Nyquist plots for formate oxidation at different potentials at pH 5 and 13 are shown in Figure 6a,b, respectively. In order to interpret the EIS results, we considered a simplified physical model for nanoporous electrodes (Figure 6c), which provides two arcs, consistently with the obtained Nyquist plots in all tested conditions. In this model, we considered that the FTO substrate (C_{FTO}) is in contact with the liquid electrolyte but does not transfer charge to the solution (as confirmed by blank experiments with bare FTO). Charge transport within the CoFePB layer is modeled through a resistor (R_t), related to film conductivity. Charge transfer at the CoFePB/solution interface is modeled by a parallel RC element ($R_{ct}/C_{CoFe\text{-}PB}$) and R_s is the series resistance, which conveys the resistance of the solution, contact, and wiring. The detailed explanation for the selection of this model can be found in the Supporting Information discussion and Figure S13.

The CoFePB films were studied by EIS in 0.4 M formate solution in different potential windows according to pH, 1.2−1.7 V *vs* RHE at pH 5 and 1.17−1.57 V *vs* RHE at pH 13, to avoid the contribution of the OER process taking place at more anodic potentials (Figure 2). In all cases, the EIS plots

Table 2. Comparison of Electrocatalytic Activity of Pd(5%)/C, Pt Disk, and CoFePB Electrodes Obtained by CV under the Conditions Shown in Figure 5, in Terms of Onset Overpotential (η_{onset}), Maximum Current Density (j_{max}) Obtained on the Forward Scan (at an η_{peak}), and Current Density (j) Obtained at Given η

			j/(mA cm^{-2})		
catalyst	η_{onset}/V	j_{max}/ (mA cm^{-2})	η = 1.2 V	η = 1.4 V	η = 1.6 V
Pd/C (pH 5)	0.3	0.6 (at 0.8 V)	0.5	0.7	1.4
Pt (pH 5)	0.5	0.5 (at 1.6 V)	0.3	0.3	0.4
CoFePB (pH 5)	1.4	10.1		0.2	10.1
Pd/C (pH 13)	0.4	3.3 (at 0.9 V)	2.4	2.2	1.9
Pt (pH 13)	0.7	3.1 (at 1.3 V)	2.1	2.0	0.9
CoFePB (pH 13)	1.4	6.0		0.3	6.0

https://dx.doi.org/10.1021/acsaem.0c01548
ACS Appl. Energy Mater. 2020, 3, 9198−9207

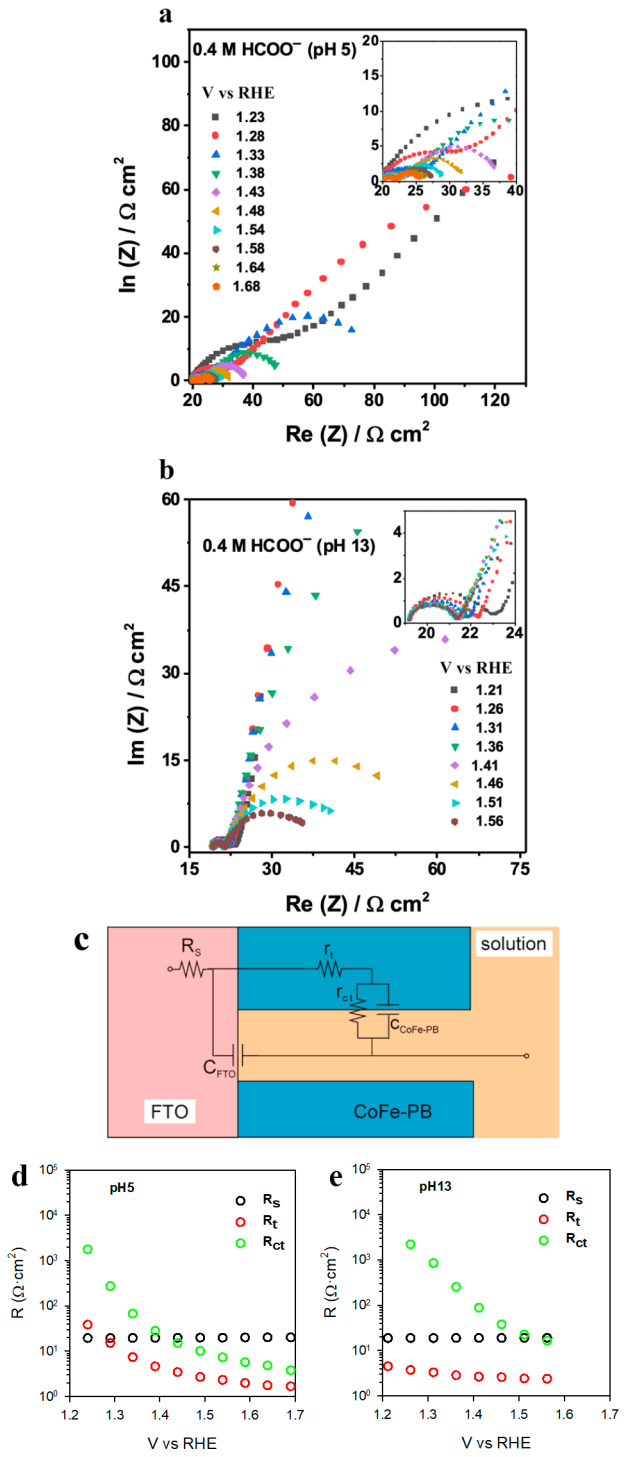

Figure 6. EIS data for CoFePB electrodes. Representative Nyquist plots for formate oxidation at (a) pH 5 or (b) pH 13. (c) Equivalent circuit employed to fit the experimental impedance data. (d) Resistances extracted from the Nyquist plots at pH 5 for formate oxidation. (e) Resistances extracted from the Nyquist plots at pH 13 for formate oxidation. Series resistance (R_s), charge transfer resistance (R_{ct}), and transport resistance (R_t) are shown in black, green, and red, respectively.

showed two well-defined semicircles confined in the first quadrant. At pH 5, the low-frequency loop exhibits a Tafel slope of 69 mV·dec^{-1} (Figure S14), in good agreement with the chronoamperometric measurements (Figure S12a). This supports the assignment of this low-frequency loop to the charge transfer process occurring at the CoFePB/solution interface during formate oxidation. At both pH 5 and pH 13 the arc diameter decreases when potential is increased. This is in contrast to the case of electrooxidation on precious metal electrocatalysts, where a negative Faradaic impedance appears due to the oxidative removal of passivating CO_{ads} that blocks active sites.[18,51,52] This supports again the absence of CO production and/or CO passivation in the case of our CoFePB films. At both pH conditions, the high-frequency arc diameter also decreases when increasing the applied potentials. We associated this arc to the charge transport process across the CoFePB film, a semiconductor with strong charge localization.[53,54] This hypothesis is in good agreement with the EIS data obtained with a CoFePB film in aqueous solution in the absence of formate (Figures S15 and S16). The charge transport kinetics for formate oxidation decreases with applied potential down to the anodic reversible Co^{2+}/Co^{3+} redox event at both pHs and then remains constant at higher potentials (Figures 6d,e and S16a).

By comparison with the electrode performance in the absence of formate, only one depressed high-frequency semicircle followed by a quasi-vertical line (pure capacitance reflecting a blocking interface) is observed at pH 5 in the potential window of 1.2−1.7 V *vs* RHE. This confirms the poor catalytic activity of CoFePB for water oxidation in the formate oxidation potential range and confirms that formate oxidation is the only significant redox event at pH 5. At pH 13, the charge transfer resistance that we assign to water oxidation is delayed around 300 mV compared to that for formate oxidation, also reflecting that formate oxidation is still the dominant process in the potential window studied (Figure S16b). Finally, R_s is identical for both water oxidation and formate oxidation, as expected (Figure S16c). The extracted capacitiances are consistent with the above interpretation (Figure S17). Indeed, the high capacitances of the CoFePB layer (around 10^{-2}−10^{-1} F·cm^{-2}) are consistent with a highly porous layer, with a contribution from redox events, such as Co^{2+}/Co^{3+}. Also, the values for C_{FTO} are qualitatively in good agreement with the blank measurements carried out on bare FTO substrate in contact with the solution.

Hole transfer to the solution is the limiting step for formate oxidation at low overpotentials, between 1.2 and 1.45 V *vs* RHE at pH 5 and between 1.17 and 1.57 V *vs* RHE at pH 13 (since R_{ct} is tha highest circuit resistance). Conversely, at more anodic applied potentials the series resistance becomes the limiting factor, which can be mainly ascribed to the electrolyte conductivity, apart from connections and wiring. This suggests that device engineering must be improved, targeting technological applications of CoFePB electrodes.

CONCLUSIONS

In this work, we have disclosed the activity of the Co−Fe Prussian Blue derivative to catalyze the oxidation of formate and formic acid in aqueous solutions. This catalyst offers quantitative selectivity toward CO_2 with Faradaic efficiency near 100% and is active in the pH 1−13 range. CoFePB is selective toward formate oxidation, whereas methanol, ethanol, acetate, and water are all oxidized at much higher overpotentials. Long-term experiments and postcatalysis characterization provide evidence supporting the high stability of CoFePB and, importantly, the absence of other species that are catalytically active toward formate oxidation—thereby implying that CoFePB is the true catalytically active species. Control

https://dx.doi.org/10.1021/acsaem.0c01548
ACS Appl. Energy Mater. 2020, 3, 9198−9207

experiments with state-of-the-art Pt and Pd(5%)/C show that although the noble metal catalysts are poisoned by adsorbed intermediates at high current density, CoFePB remains active and is able to achieve stable current densities outperforming its noble metal competitors. Charge transport and charge transfer steps have been identified by EIS, hole transfer being the limiting factor for formate oxidation at moderate applied potentials, and reveal that device engineering should be optimized for relevant technological appilcations in formate fuel cell devices and/or formate sensors.

■ ASSOCIATED CONTENT

Supporting Information

The Supporting Information is available free of charge at https://pubs.acs.org/doi/10.1021/acsaem.0c01548.

Additional electrochemical data; composition and structural characterization by IR and Raman, STEM, EELS, NMR, and MS analyses (PDF)

■ AUTHOR INFORMATION

Corresponding Author

Jose Ramon Galan-Mascaros − *Institute of Chemical Research of Catalonia (ICIQ), The Barcelona Institute of Science and Technology (BIST), 43007 Tarragona, Spain; ICREA, 08010 Barcelona, Spain;* orcid.org/0000-0001-7983-9762; Email: jrgalan@iciq.es

Authors

Lijuan Han − *Institute of Chemical Research of Catalonia (ICIQ), The Barcelona Institute of Science and Technology (BIST), 43007 Tarragona, Spain*

Jesús González-Cobos − *Institute of Chemical Research of Catalonia (ICIQ), The Barcelona Institute of Science and Technology (BIST), 43007 Tarragona, Spain;* orcid.org/0000-0003-0885-5815

Irene Sánchez-Molina − *Institute of Chemical Research of Catalonia (ICIQ), The Barcelona Institute of Science and Technology (BIST), 43007 Tarragona, Spain*

Stefano Giancola − *Institute of Chemical Research of Catalonia (ICIQ), The Barcelona Institute of Science and Technology (BIST), 43007 Tarragona, Spain*

Scott J. Folkman − *Institute of Chemical Research of Catalonia (ICIQ), The Barcelona Institute of Science and Technology (BIST), 43007 Tarragona, Spain;* orcid.org/0000-0002-8124-7253

Pengyi Tang − *Catalan Institute of Nanoscience and Nanotechnology (ICN2), CSIC and BIST, 08193 Barcelona, Catalonia, Spain*

Marc Heggen − *Ernst-Ruska Centre for Microscopy and Spectroscopy with Electrons and Peter Grünberg Institute, Forschungszentrum Jülich GmbH, 52425 Jülich, Germany;* orcid.org/0000-0002-2646-0078

Rafal E. Dunin-Borkowski − *Ernst-Ruska Centre for Microscopy and Spectroscopy with Electrons and Peter Grünberg Institute, Forschungszentrum Jülich GmbH, 52425 Jülich, Germany;* orcid.org/0000-0001-8082-0647

Jordi Arbiol − *Catalan Institute of Nanoscience and Nanotechnology (ICN2), CSIC and BIST, 08193 Barcelona, Catalonia, Spain; ICREA, 08010 Barcelona, Spain;* orcid.org/0000-0002-0695-1726

Sixto Giménez − *Institute of Advanced Materials (INAM), Universitat Jaume I, 12006 Castelló, Spain;* orcid.org/0000-0002-4522-3174

Complete contact information is available at: https://pubs.acs.org/10.1021/acsaem.0c01548

Notes

The authors declare no competing financial interest.

■ ACKNOWLEDGMENTS

We thank Dr. Hong-Chu Du and Dr. Paul Paciok from the Ernst-Ruska Centre for Microscopy and Spectroscopy with Electrons for their contribution in high-angle annular dark-field (HAADF)-STEM and EELS characterization. We acknowledge Prof. Julio Lloret-Fillol and Sergio Fernández from ICIQ for their helpful discussion. We gratefully acknowledge financial support from the FEDER/Ministerio de Ciencia e Innovación−Agencia Estatal de Investigación through Projects RTI2018-095618-B-I00 and ENE2017-85087-C3; the Generalitat de Catalunya (Grant Nos. 2017-SGR-1406 and 2017-SGR-327), and the CERCA Programme/Generalitat de Catalunya. I.S.-M. thanks the Marie Skłodowska-Curie COFUND program PRO-BIST for her postdoctoral contract (Grant Agreement No. 754510). ICN2 is supported by the Severo Ochoa program from Spanish MINECO (Grant No. SEV-2017-0706). ICN2 and ICIQ acknowledge funding from the BIST Ignite Project InWOC2.

■ REFERENCES

(1) An, L.; Chen, R. Direct formate fuel cells: A review. *J. Power Sources* **2016**, *320*, 127.

(2) Singh, A. K.; Singh, S.; Kumar, A. Hydrogen energy future with formic acid: A renewable chemical hydrogen storage system. *Catal. Sci. Technol.* **2016**, *6*, 12.

(3) Mansor, M.; Timmiati, S. N.; Lim, K. L.; Wong, W. Y.; Kamarudin, S. K.; Nazirah Kamarudin, N. H. Recent progress of anode catalysts and their support materials for methanol electro-oxidation reaction. *Int. J. Hydrogen Energy* **2019**, *44*, 14744.

(4) Monyoncho, E. A.; Woo, T. K.; Baranova, E. A. *SPR Electrochemistry*; Royal Society of Chemistry: Cambridge, U.K., 2019; Vol. *15*, p 1, DOI: 10.1039/9781788013895.

(5) González-Cobos, J.; Baranton, S.; Coutanceau, C. Development of Bismuth-Modified PtPd Nanocatalysts for the Electrochemical Reforming of Polyols into Hydrogen and Value-Added Chemicals. *ChemElectroChem* **2016**, *3*, 1694.

(6) Caravaca, A.; Garcia-Lorefice, W. E.; Gil, S.; de Lucas-Consuegra, A.; Vernoux, P. Towards a sustainable technology for H 2 production: Direct lignin electrolysis in a continuous-flow Polymer Electrolyte Membrane reactor. *Electrochem. Commun.* **2019**, *100*, 43.

(7) Waldie, K. M.; Brunner, F. M.; Kubiak, C. P. Transition Metal Hydride Catalysts for Sustainable Interconversion of CO_2 and Formate: Thermodynamic and Mechanistic Considerations. *ACS Sustainable Chem. Eng.* **2018**, *6*, 6841.

(8) Lu, X.; Wu, Y.; Yuan, X.; Wang, H. An Integrated CO2 Electrolyzer and Formate Fuel Cell Enabled by a Reversibly Restructuring Pb−Pd Bimetallic Catalyst. *Angew. Chem., Int. Ed.* **2019**, *58*, 4031.

(9) Pilas, J.; Yazici, Y.; Selmer, T.; Keusgen, M.; Schöning, M. J. Optimization of an amperometric biosensor array for simultaneous measurement of ethanol, formate, d- and l-lactate. *Electrochim. Acta* **2017**, *251*, 256.

(10) Röhlen, D. L.; Pilas, J.; Dahmen, M.; Keusgen, M.; Selmer, T.; Schöning, M. J. Toward a Hybrid Biosensor System for Analysis of Organic and Volatile Fatty Acids in Fermentation Processes. *Front. Chem.* **2018**, *6*, 284.

(11) Daniele, S.; Bragato, C.; Battistel, D. Bismuth-Coated Mesoporous Platinum Microelectrodes as Sensors for Formic Acid Detection. *Electroanalysis* **2012**, *24*, 759.
(12) Mak, K. K. W.; Wollenberger, U.; Scheller, F. W.; Renneberg, R. An amperometric bi-enzyme sensor for determination of formate using cofactor regeneration. *Biosens. Bioelectron.* **2003**, *18*, 1095.
(13) Soloveichik, G. L. Liquid fuel cells. *Beilstein J. Nanotechnol.* **2014**, *5*, 1399.
(14) Ong, B. C.; Kamarudin, S. K.; Basri, S. Direct liquid fuel cells: A review. *Int. J. Hydrogen Energy* **2017**, *42*, 10142.
(15) Yu, X.; Pickup, P. G. Recent advances in direct formic acid fuel cells (DFAFC). *J. Power Sources* **2008**, *182*, 124.
(16) Douk, A. S.; Farsadrooh, M.; Damanigol, F.; Moghaddam, A. A.; Saravani, H.; Noroozifar, M. Porous three-dimensional network of Pd−Cu aerogel toward formic acid oxidation. *RSC Adv.* **2018**, *8*, 23539.
(17) Xi, Z.; Li, J.; Su, D.; Muzzio, M.; Yu, C.; Li, Q.; Sun, S. Stabilizing CuPd Nanoparticles via CuPd Coupling to $WO_{2.72}$ Nanorods in Electrochemical Oxidation of Formic Acid. *J. Am. Chem. Soc.* **2017**, *139*, 15191.
(18) Chen, W.; Kim, J.; Sun, S.; Chen, S. Electro-oxidation of formic acid catalyzed by FePt nanoparticles. *Phys. Chem. Chem. Phys.* **2006**, *8*, 2779.
(19) Sankar, S.; Anilkumar, G. M.; Tamaki, T.; Yamaguchi, T. Binary Pd−Ni Nanoalloy Particles over Carbon Support with Superior Alkaline Formate Fuel Electrooxidation Performance. *ChemCatChem* **2019**, *11*, 4731.
(20) Bisht, A.; Pentyala, P.; Deshpande, P. A.; Sharma, S. $La_{0.80}Sr_{0.20}CoO_3$ as a noble-metal-free catalyst for the direct oxidation of formic acid under zero applied potential. *Electrochem. Commun.* **2019**, *99*, 1.
(21) Cracknell, J. A.; Vincent, K. A.; Armstrong, F. A. Enzymes as Working or Inspirational Electrocatalysts for Fuel Cells and Electrolysis. *Chem. Rev.* **2008**, *108*, 2439.
(22) Robinson, W. E.; Bassegoda, A.; Reisner, E.; Hirst, J. Oxidation-State-Dependent Binding Properties of the Active Site in a Mo-Containing Formate Dehydrogenase. *J. Am. Chem. Soc.* **2017**, *139*, 9927.
(23) Galan, B. R.; Schöffel, J.; Linehan, J. C.; Seu, C.; Appel, A. M.; Roberts, J. A. S.; Helm, M. L.; Kilgore, U. J.; Yang, J. Y.; DuBois, D. L.; Kubiak, C. P. Electrocatalytic Oxidation of Formate by $[Ni(PR_2NR'_2)_2(CH_3CN)]^{2+}$ Complexes. *J. Am. Chem. Soc.* **2011**, *133*, 12767.
(24) Seu, C. S.; Appel, A. M.; Doud, M. D.; DuBois, D. L.; Kubiak, C. P. Formate oxidation via β-deprotonation in $[Ni(PR_2NR'_2)_2(CH_3CN)]^{2+}$ complexes. *Energy Environ. Sci.* **2012**, *5*, 6480.
(25) Han, L.; Tang, P.; Reyes-Carmona, Á.; Rodríguez-García, B.; Torréns, M.; Morante, J. R.; Arbiol, J.; Galan-Mascaros, J. R. Enhanced Activity and Acid pH Stability of Prussian Blue-type Oxygen Evolution Electrocatalysts Processed by Chemical Etching. *J. Am. Chem. Soc.* **2016**, *138*, 16037.
(26) Rodríguez-García, B.; Reyes-Carmona, Á.; Jiménez-Morales, I.; Blasco-Ahicart, M.; Cavaliere, S.; Dupont, M.; Jones, D.; Rozière, J.; Galán-Mascarós, J. R.; Jaouen, F. Cobalt hexacyanoferrate supported on Sb-doped SnO_2 as a non-noble catalyst for oxygen evolution in acidic medium. *Sustainable Energy Fuels* **2018**, *2*, 589.
(27) Garcés-Pineda, F. A.; González-Cobos, J.; Torrens, M.; Galán-Mascarós, J. R. Fluorine-Doped Tin Oxide/Alumina as Long-Term Robust Conducting Support for Earth-Abundant Water Oxidation Electrocatalysts. *ChemElectroChem* **2019**, *6*, 2282.
(28) Goberna-Ferrón, S.; Hernández, W. Y.; Rodríguez-García, B.; Galán-Mascarós, J. R. Light-driven water oxidation with metal hexacyanometallate heterogeneous catalysts. *ACS Catal.* **2014**, *4*, 1637.
(29) Choun, M.; Ham, K.; Shin, D.; Lee, J. K.; Lee, J. Catalytically active highly metallic palladium on carbon support for oxidation of $HCOO^-$. *Catal. Today* **2017**, *295*, 26.
(30) Joo, J.; Choun, M.; Jeong, J.; Lee, J. Influence of Solution pH on Pt Anode Catalyst in Direct Formic Acid Fuel Cells. *ACS Catal.* **2015**, *5*, 6848.
(31) Joo, J.; Uchida, T.; Cuesta, A.; Koper, M. T. M.; Osawa, M. The effect of pH on the electrocatalytic oxidation of formic acid/formate on platinum: A mechanistic study by surface-enhanced infrared spectroscopy coupled with cyclic voltammetry. *Electrochim. Acta* **2014**, *129*, 127.
(32) Brimaud, S.; Solla-Gullón, J.; Weber, I.; Feliu, J. M.; Behm, R. J. Formic Acid Electrooxidation on Noble-Metal Electrodes: Role and Mechanistic Implications of pH, Surface Structure, and Anion Adsorption. *ChemElectroChem* **2014**, *1*, 1075.
(33) Perales-Rondón, J. V.; Brimaud, S.; Solla-Gullón, J.; Herrero, E.; Jürgen Behm, R.; Feliu, J. M. Further Insights into the Formic Acid Oxidation Mechanism on Platinum: pH and Anion Adsorption Effects. *Electrochim. Acta* **2015**, *180*, 479.
(34) Okamoto, H.; Kon, W.; Mukouyama, Y. Stationary Voltammogram for Oxidation of Formic Acid on Polycrystalline Platinum. *J. Phys. Chem. B* **2004**, *108*, 4432.
(35) Hong, J. W.; Kim, D.; Lee, Y. W.; Kim, M.; Kang, S. W.; Han, S. W. Atomic-distribution-dependent electrocatalytic activity of Au-Pd bimetallic nanocrystals. *Angew. Chem., Int. Ed.* **2011**, *50*, 8876.
(36) Nonaka, H.; Matsumura, Y. Electrochemical oxidation of carbon monoxide, methanol, formic acid, ethanol, and acetic acid on a platinum electrode under hot aqueous conditions. *J. Electroanal. Chem.* **2002**, *520*, 101.
(37) Wang, X.; Wang, W.; Qi, Z.; Zhao, C.; Ji, H.; Zhang, Z. High catalytic activity of ultrafine nanoporous palladium for electro-oxidation of methanol, ethanol, and formic acid. *Electrochem. Commun.* **2009**, *11*, 1896.
(38) Hsieh, C.-T.; Hsiao, H.-T.; Tzou, D.-Y.; Yu, P.-Y.; Chen, P.-Y.; Jang, B.-S. Electro-oxidation of methanol and formic acid on platinum nanoparticles with different oxidation levels. *Mater. Chem. Phys.* **2015**, *149−150*, 359.
(39) Yu, X.; Manthiram, A. Catalyst-selective, scalable membraneless alkaline direct formate fuel cells. *Appl. Catal., B* **2015**, *165*, 63.
(40) Alsac, E. P.; Ulker, E.; Nune, S. V. K.; Dede, Y.; Karadas, F. Tuning the Electronic Properties of Prussian Blue Analogues for Efficient Water Oxidation Electrocatalysis: Experimental and Computational Studies. *Chem. - Eur. J.* **2018**, *24*, 4856.
(41) Aksoy, M.; Nune, S. V. K.; Karadas, F. A Novel Synthetic Route for the Preparation of an Amorphous Co/Fe Prussian Blue Coordination Compound with High Electrocatalytic Water Oxidation Activity. *Inorg. Chem.* **2016**, *55*, 4301.
(42) Stracke, J. J.; Finke, R. G. Electrocatalytic Water Oxidation Beginning with the Cobalt Polyoxometalate $[Co_4(H_2O)_2(PW_9O_{34})_2]^{10-}$: Identification of Heterogeneous CoO_x as the Dominant Catalyst. *J. Am. Chem. Soc.* **2011**, *133*, 14872.
(43) Ullman, A. M.; Liu, Y.; Huynh, M.; Bediako, D. K.; Wang, H.; Anderson, B. L.; Powers, D. C.; Breen, J. J.; Abruña, H. D.; Nocera, D. G. Water Oxidation Catalysis by Co(II) Impurities in $Co(III)_4O_4$ Cubanes. *J. Am. Chem. Soc.* **2014**, *136*, 17681.
(44) Burke, M. S.; Kast, M. G.; Trotochaud, L.; Smith, A. M.; Boettcher, S. W. Cobalt−Iron (Oxy)hydroxide Oxygen Evolution Electrocatalysts: The Role of Structure and Composition on Activity, Stability, and Mechanism. *J. Am. Chem. Soc.* **2015**, *137*, 3638.
(45) Folkman, S. J.; Soriano-Lopez, J.; Galán-Mascarós, J. R.; Finke, R. G. Electrochemically Driven Water-Oxidation Catalysis Beginning with Six Exemplary Cobalt Polyoxometalates: Is It Molecular, Homogeneous Catalysis or Electrode-Bound, Heterogeneous CoO_x Catalysis? *J. Am. Chem. Soc.* **2018**, *140*, 12040.
(46) Jeong, S.; Shin, W. Triple-pulse Method for Monitoring Formate in CO2 Conversion Process. *Electroanalysis* **2016**, *28*, 1437.
(47) Jiang, J.; Scott, J.; Wieckowski, A. Direct evidence of a triple-path mechanism of formate electrooxidation on Pt black in alkaline media at varying temperature. Part I: The electrochemical studies. *Electrochim. Acta* **2013**, *104*, 124.
(48) Wang, J.; Liu, C.; Banis, M. N.; Cheng, N.; Riese, A.; Wang, S.; Sun, X. Superior anti-poisoning performance of graphenes versus

https://dx.doi.org/10.1021/acsaem.0c01548
ACS Appl. Energy Mater. 2020, 3, 9198−9207

carbon nanotubes as Pt catalysts supports for formate oxidation. *Int. J. Hydrogen Energy* **2016**, *41*, 936.
(49) Yépez, O.; Scharifker, B. R. Oxidation of formate on hydrogen-loaded palladium. *Int. J. Hydrogen Energy* **2002**, *27*, 99.
(50) Pletcher, D. *A First Course in Electrode Processes*, 2nd ed.; Royal Society of Chemistry: Cambridge, U.K., 2009.
(51) Lu, Y.; Chen, W. Nanoneedle-covered Pd-Ag nanotubes: High electrocatalytic activity for formic acid oxidation. *J. Phys. Chem. C* **2010**, *114*, 21190.
(52) Lu, Y.; Chen, W. PdAg alloy nanowires: Facile one-step synthesis and high electrocatalytic activity for formic acid oxidation. *ACS Catal.* **2012**, *2*, 84.
(53) García-Jareño, J. J.; Navarro, J. J.; Roig, A. F.; Scholl, H.; Vicente, F. Impedance analysis of Prussian Blue films deposited on ITO electrodes. *Electrochim. Acta* **1995**, *40*, 1113.
(54) García-Jareño, J. J.; Navarro-Laboulais, J.; Vicente, F. Charge transport in Prussian Blue films deposited on ITO electrodes. *Electrochim. Acta* **1996**, *41*, 835.

https://dx.doi.org/10.1021/acsaem.0c01548
ACS Appl. Energy Mater. 2020, 3, 9198−9207